University of Glasgow

DEPARTMENT OF

AEROSPACE ENGINEERING

mulation of Parallel Blade-Vortex Interaction using a Discrete Vortex Method.

by

L. Qian and M. Vezza

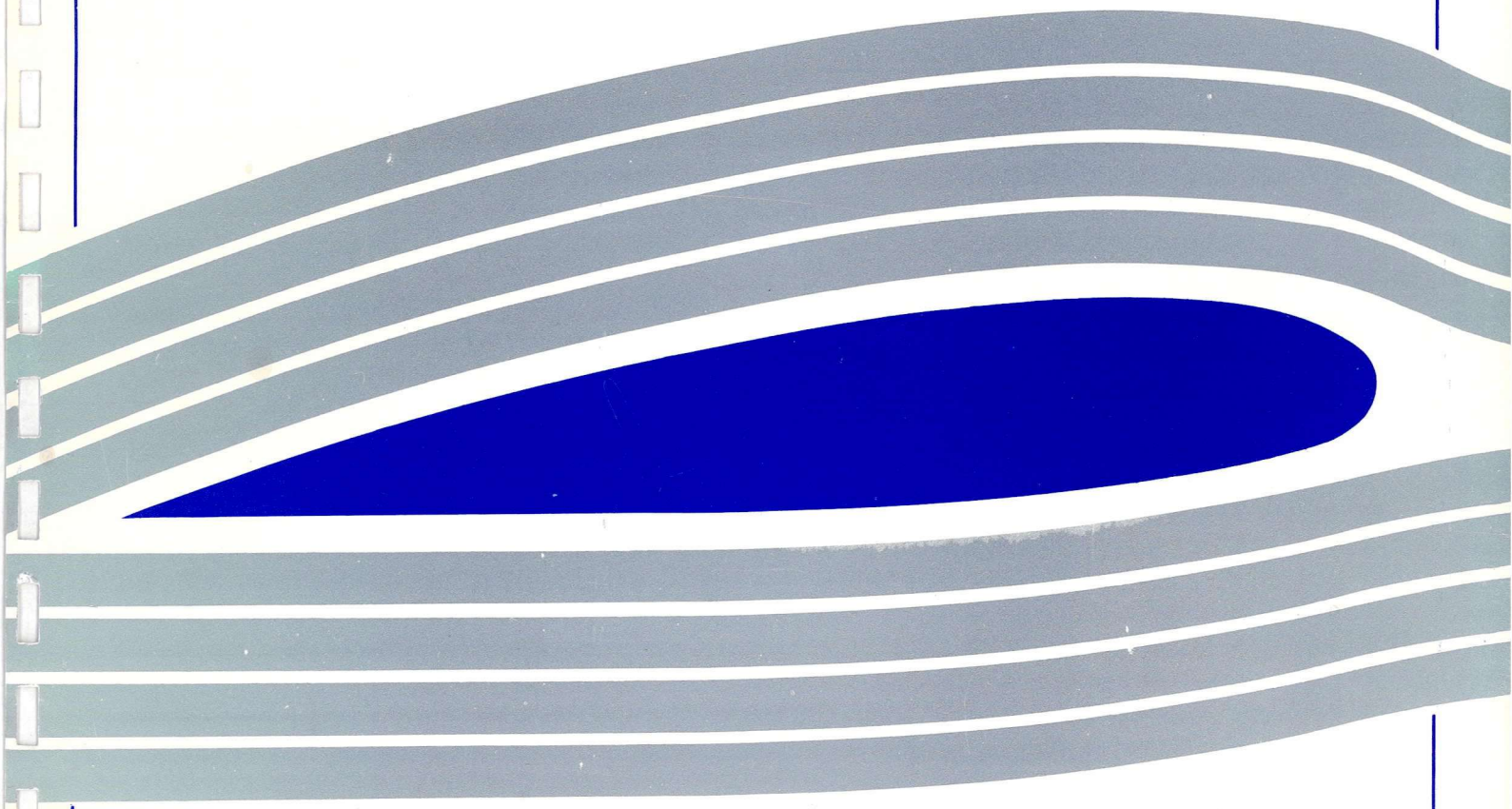

UNIVERSITY
of
GLASGOW

Simulation of Parallel Blade-Vortex Interaction using a Discrete Vortex Method.

by

L. Qian and M. Vezza

Department of Aerospace Engineering
University of Glasgow
Glasgow G12 8QQ.

G.U. Aero Report No. 9832
November 1998.

Simulation of Parallel Blade-Vortex Interaction using a Discrete Vortex Method

Ling Qian and Marco Vezza

Abstract.
Numerical results are presented for two-dimensional vortex-aerofoil interaction using a grid-free discrete vortex method. The effects of the passing vortex on the surface pressure distribution and hence the aerodynamic force and moment of the aerofoil are examined in detail for a variety of interaction geometries. For some head-on interaction cases, vortex-induced local flow separation is also predicted on the aft part of the aerofoil surfaces. Extensive comparisons are made with other numerical results and the results from the Glasgow University BVI wind-tunnel test, which show good agreement.

Nomenclature.

c	Blade chord length
$C_{m\frac{1}{4}}$	Quarter-chord moment coefficient
C_n	Normal force coefficient
C_t	Tangential force coefficient
h	Height of the control zone
N_s	Number of nascent vortices in each panel
p	Pressure
r	Radial position of pressure measurement pod
R	Rotor blade radius
Re	Reynolds number
$(\vec{s},\vec{n})$	Unit vector of the local surface coordinate system
t	Time
$\vec{u}$	Velocity
$\vec{u}_\infty$	Velocity of the free stream (u_∞,v_∞)
$\vec{x}$	Position vector (x,y)
(X_v,Y_v)	Initial position of the interation vortex
σ	Core radius of the vortex particles
ω	Vorticity
Γ_j	Circulation of vortex particle j
Γ_v	Circulation of the interaction vortex
Ψ	Stream function
Δs	Length of each panel

1 INTRODUCTION

Blade-vortex interaction (BVI) in the flow field about helicopter rotors is a phenomenon in which the rotor blade passes through the tip vortices shed from preceding blades. The interaction can occur in forward flight, but more often occurs during manoeuvres and vertical descent, and is most severe when the vortex approaches the blade approximately aligned with the spanwise axis of the blade (parallel interaction). The BVI event not only drastically changes the aerodynamic loads on the rotor, but is also one of the sources of helicopter noise and vibration. During the last two decades, a number of experimental studies have been done in an attempt to gain a clear understanding of the fluid dynamic mechanisms behind the BVI phenomenon [1][2]. In particular, at Glasgow University, a series of parallel BVI data have been

collected and archived as a result of an experimental research programme [3][4][5], providing a useful validation tool for analytic and numerical schemes.

Meanwhile, some numerical studies on BVI have also been carried out, mainly based on the unsteady panel method and conformal mapping method [6]. In the early studies, a point vortex [7][8] was used to represent the interaction vortex, and its influence on the aerodynamic force exerted on the aerofoil was given. More recently, the distributed vortex model [9][10][11], in which the finite core of the vortex was discretised into multiple vortex elements or particles, was employed to examine the effects of the vortex deformation and splitting during a close interaction. However, these methods, which were derived from the theory of potential flow, have been restricted by shedding vorticity from the trailing edge only, using the unsteady Kutta condition, thereby precluding vortex-induced flow separation and interaction at a high angle of incidence. Among others, the grid-based finite difference method has also been used. In [12], the incompressible Navier-Stokes equations were solved for the 2-D BVI problem for Reynolds numbers less than 200. Later, to reduce the excessive numerical diffusion of the interaction vortex, a high-order space discretisation scheme was applied for the convection term in the thin-layer N-S equations [13]. In [14], a 2-D full potential model was also used to model parallel BVI in the transonic flow regime. However as stated in a recent review of helicopter aerodynamics [15], the grid-based methods currently still suffer from difficulties in capturing and subsquently tracking compact vorticity regions, such as the interaction vortex, unless more complicated and time-consuming high order space discretisation schemes and self-adaptive grid generation systems are used.

In the present study, the grid-free vortex method [16][17] is employed to study the two dimensional blade-vortex interaction problem shown in figure 1. The entire vorticity region including the oncoming vortex is represented by a finite number of vortex blobs (particles with finite core radius) which are tracked through the flow according to the local velocity calculated from the Biot-Savart law. The effect of viscous diffusion is modelled by the random walk method. The boundary condition at the aerofoil surface is satisfied at each-time step by introducing new vortices along the surface which are, in part or in whole, allowed to enter the wake from the entire surface. The method thus avoids the need for either a Kutta condition to determine vorticity shedding rate or empirical methods to calculate flow separation points. The flexibility and robustness of the method make it possible to examine a wide range of BVI cases which, in conjunction with the experimental tests, contributes to a better understanding of the mechanisms of BVI.

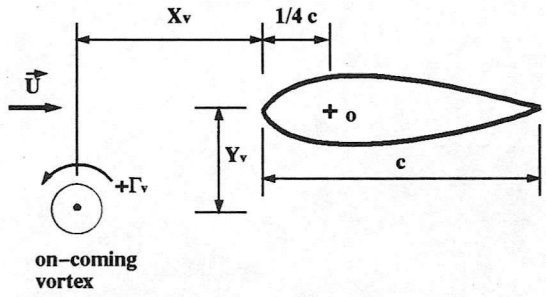

Figure 1. Parallel blade-vortex interaction

In the following sections, the theoretical background of the vortex method is reviewed, followed by a detailed description of the numerical implementation. By examining and comparing the numerical results for a number of interaction cases with those obtained from other numerical and experimental studies, the mechanisms of the BVI event are analysed. Finally, a brief discussion of future work is given.

2 MATHEMATICAL FORMULATION

Two-dimensional incompressible viscous flow can be described by the vorticity(ω)-stream function(ψ) form of the Navier-Stokes equations together with the boundary conditions, which consist of::

vorticity transport equation:

$$\frac{d\omega}{dt}=\frac{\partial\omega}{\partial t}+\vec{u}\cdot\nabla\omega=\nu\nabla^2\omega \tag{1}$$

continuity equation:

$$\nabla^2\psi=-\omega \tag{2}$$

far-field boundary condition:

$$\vec{u}=\vec{u}_\infty \text{ or } \nabla\psi=\nabla\psi_\infty \tag{3}$$

and the no-slip and no penetration conditions at the surface of a stationary body:

$$\vec{u}=\vec{u}_b(\vec{x}_s,t)=0 \text{ or } \nabla\psi=\nabla\psi_b(\vec{x}_s,t)=0 \tag{4}$$

The Poisson equation for ψ can be solved in terms of ω by using Green's identity and the boundary conditions given in eq.(3) and eq.(4), which gives

$$\psi(\vec{x},t)=-\frac{1}{2\pi}\int_D ln|\vec{x}-\vec{x}'|\omega(\vec{x}',t)\,dS+u_\infty y-v_\infty x+c \tag{5}$$

where c is a constant. Accordingly, the velocity at any point $\vec{x}$ in the flowfield is

$$\vec{u}(\vec{x},t)=\frac{1}{2\pi}\int_D\frac{\omega(\vec{x}',t)\vec{k}\times(\vec{x}-\vec{x}')}{|\vec{x}-\vec{x}'|^2}\,dS+\vec{u}_\infty \tag{6}$$

where the integral over area D in both eq.(5) and eq.(6) is taken over the portion of the fluid region containing non-zero vorticity. Eq.(6) is a particular application of the Biot-Savart Law.

Based on eq.(1) and eq.(5) or eq.(6), which represent the kinetic and kinematic aspects of the entire flow problem respectively, vorticity based methods, including discrete vortex methods, can be constructed. For unbounded flow problems, only the initial distribution of the vorticity is needed for its subsquent development. For bounded flow, however, the fact that vorticity will be created at the body surface should be taken into account. In the present method this is achieved by splitting the area integral in eq.(5) or eq.(6) into two parts:

$$\psi(\vec{x},t)=-\frac{1}{2\pi}\int_{D'+D''} ln|\vec{x}-\vec{x}'|\omega(\vec{x}',t)\,dS+u_\infty y-v_\infty x+c \tag{7}$$

and

$$\vec{u}(\vec{x},t)=\frac{1}{2\pi}\int_{D'+D''}\frac{\omega(\vec{x}',t)\vec{k}\times(\vec{x}-\vec{x}')}{|\vec{x}-\vec{x}'|^2}\,dS+\vec{u}_\infty \tag{8}$$

where the zone D' is a thin strip encompassing the body surface, while the zone D'' is the rest of the integral area D. For each time-step, the vorticity (or circulation) distribution in zone D', which includes both vorticity newly generated during the timestep and the residual vorticity from the previous timestep, is calculated by satisfying the boundary conditions. In the context of vortex methods, it can be shown [17] that the no-slip condition and the no-penetration condition are equivalent. In the present study, only the no-penetration condition is used, which will be discussed in detail later.

3 NUMERICAL IMPLEMENTATION - DISCRETE VORTEX METHOD

3.1 Discretisation and evolution of the vorticity field

In the discrete vortex method, the continuous vorticity field is approximated by a set of overlapping vortex blobs (particles with a finite core radius σ):

$$\omega(\vec{x})=\sum_{j=1}^{N}\Gamma_j\delta_\sigma(\vec{x}-\vec{x}_j) \tag{9}$$

where Γ_j is the strength (circulation) of the vortex particle located at $\vec{x}_j$ and the smooth core function $\delta_\sigma(\vec{x}-\vec{x}_j)$ is usually radially symmetric, i.e. $\delta_\sigma(\vec{x}-\vec{x}_j)=\frac{1}{\sigma^2}f(\frac{|\vec{x}-\vec{x}_j|}{\sigma})$ and $2\pi\int_0^\infty rf(r)\,dr=1$. Although a number of choices are available in selecting the core function, such as the Gaussian and Rankine models, a simple vortex model, which is usually referred to as the Scully model with $f(r)=\frac{1}{\pi}\frac{1}{(r^2+1)^2}$ has been implemented.

In accordance with the vorticity distribution represented by eq.(9), the velocity at any point $\vec{x}$ in the flow field, particlarly at the center of each particle $\vec{x}_j$, can be calculated using the Biot-Savart law, which gives

$$\vec{u}(\vec{x})=\frac{1}{2\pi}\vec{k}\times\sum_{j=1}^{N}\Gamma_j\frac{\vec{x}-\vec{x}_j}{|\vec{x}-\vec{x}_j|}F(\frac{|\vec{x}-\vec{x}_j|}{\sigma}) \tag{10}$$

where F is defined by $F(r)=2\pi\int_0^r r'f(r')\,dr'$.

At each time step, by convecting each vortex with the local velocity using the Adams-Bashforth second order scheme and applying the random walk method [18] to mimic the effects of viscous diffusion, the new position of the vortex at $\vec{x}_j$ after time interval Δt is given by

$$\vec{x}_j(t+\Delta t)\simeq\vec{x}_j(t)+\Delta t[\frac{3}{2}\vec{u}(\vec{x}_j,t)-\frac{1}{2}\vec{u}(\vec{x}_j,t-\Delta t)]+\vec{\eta}_j \tag{11}$$

where $\vec{\eta}_j$ are a pair of independent random numbers with zero mean and variance $2\nu\Delta t$.

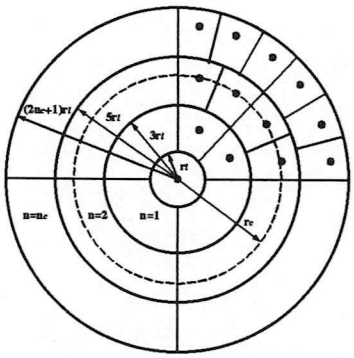

Figure 2. Discretisation of the core of the interaction vortex $r_c=r_l\frac{1+12n^2}{6n}$

For the problem of blade vortex interaction, the entire vorticity in the flow field comes from two sources: the interaction vortex which is released into the flow from the upstream of the aerofoil; the aerofoil surface where the new vorticity is created at each time step. Figure 2 shows how the initial vorticity field of the interaction vortex is discretised into a number of discrete vortex particles by overlaying the vortex with a system of patches of equal area $A=\pi r_l^2$. Each vortex particle is placed at the centroid $\vec{r}_c$ of the patch and has strength $\Gamma=\omega(\vec{r}_c)\cdot A$. The core radius of the discrete vortices ensures overlapping cores, i.e. $\sigma/r_l\geq 1$.

As far as the surface vorticity is concerned, the contour of the aerofoil is divided into a number of panels - the polygonal representation of a closed curve; and a thin strip near the body surface, which is also divided into the same number of trapezoids (control volume) as that of the panels, is set up as illustrated in figure 3. The density of the circulation $\gamma(s)=\int_0^h\omega(s,n)\,dn$, which includes both the newly generated vorticity during the current time step and the residual vorticity from the previous timestep, is assumed to vary linearly along the surface coordinate s within each control volume. The γ value at the node points (interfaces of the control zone) are unknowns. The no-penetration condition, implemented here in the zero mass flux form $\psi(\tilde{x}_{j+1})=\psi(\tilde{x}_j)$ for the panel with nodes $\tilde{x}_{j+1}$ and $\tilde{x}_j$, is enforced for each panel to determine these γ values, which leads to a linear algebraic system to be solved at each time step. However,

for N panels, it is easy to show that only $N-1$ equations are independent. A further equation is needed to make the solution unique, which is achieved by using the vorticity conservation law. For the present method, we have

$$\sum_i (\Gamma_w)_i + \sum_k (\Gamma_n)_k = \Gamma_v \tag{12}$$

where Γ_w and Γ_n are the circulations of each vortex particle in the wake and within the control zone (nascent vortices) respectively, and Γ_v is the total vorticity of the initial interaction vortex.

Once the γ values at node points are known, the vorticity in each panel is then approximated by evenly positioned and overlapping vortex particles, each of strength $\Gamma_i=\gamma(s_i)\Delta s/N_s$, i=1,2,..N_s.

Like the vortices in the wake, the vortices in the control zone are also convected and diffused at each time step. Depending on their new positions (in or out of the outer border of the control zone), they are released into the wake or absorbed as residual vorticity.

Although the velocity of the vortices in the control zone can also be calculated using eq.(10), this approach leads to an oscillating velocity distribution due to the fact that the boundary condition implemented cannot guarantee cancellation of the normal velocity at every point along the surface. The resulting transport of the vortex particles can lead to an unrealistic shedding of surface vorticity into the wake. Because the control zone is very thin, it is appropriate to assume the boundary-layer approximation there, namely $\omega = -\partial u/\partial n$, thus $\gamma(s) = -u(s)_{n=h}$. Hence the vorticity weighted average velocity across the control zone, which is also used for the tangential velocity of the nascent vortices, is given by

$$u(s)_{av} = \frac{\int_0^h u\omega\, dn}{\int_0^h \omega\, dn} = \frac{u(s)_{n=h}}{2} = -\frac{\gamma(s)}{2} \tag{13}$$

which is independent of the specific profile of $\omega(y)$. For a stationary body, using the continuity equation in each control volume, the normal velocity of the nascent vortices created above the panel with nodes j and $j+1$ is

$$(v_n)_j = \frac{\gamma_j - \gamma_{j+1}}{\Delta s}\frac{h}{2} \tag{14}$$

This is consistent with the γ distribution within the control zone and the exact boundary condition at the body surface, hence there is no oscillation within each panel.

3.2 Calculation of the surface pressure

Of particular interest in the study is an examination of the effect of the interaction vortex on the aerodynamic performance of the aerofoil, which requires the calculation of the surface pressure distribution. This, in turn, can be integrated into the aerodynamic coefficents such as C_l,C_t and $C_{m\frac{1}{4}}$.

For the body-oriented local orthogonal coordinate system $(\vec{s},\vec{n})$, the tangential momentum equation can be written at the surface of a stationary body:

$$\frac{1}{\rho}\frac{\partial p}{\partial s} = -\nu\vec{s}\cdot(\nabla\times\vec{\omega}) \tag{15}$$

which can be reduced to

$$\frac{1}{\rho}\frac{\partial p}{\partial s} = -\nu\frac{\partial \omega}{\partial n} \tag{16}$$

The term on the right-hand side of the equation represents the rate of vorticity creation per unit length at the body surface[17].

Considering a control volume with node points j and $j+1$ shown in figure 3 , the circulation at time $t-\Delta t$ is assumed to be $\gamma'\Delta s$. After convection and diffusion through the interfaces (not

including the new vorticity generated at the body surface) during a time interval Δt, which is represented by the symbols $\longrightarrow$ and $\longleftrightarrow$ respectively, the residual circulation will be $\gamma"\Delta s$. If the circulation of nascent vortices in the control volume at time t is calculated as $\gamma\Delta s$, then the newly created circulation from the body surface during the time interval Δt should be $\gamma\Delta s - \gamma"\Delta s$. Thus for this panel we have

$$\frac{p_j - p_{j+1}}{\Delta s} = \frac{\gamma - \gamma"}{\Delta t} \tag{17}$$

Once the pressure value at a reference point is known, the entire pressure distribution along the body surface can be easily calculated by integrating eq(16).

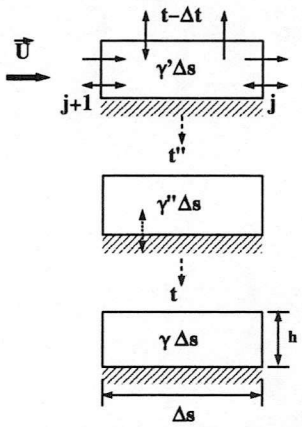

Figure 3. Surface pressure calculation

3.3 Controlling the total number of particles

The computational cost of evaluating the velocity of the system of vortices using the Biot-Savart Law is proportional to the square of the number of vortices ($O(N_v^2)$). Therefore when the total number of vortices in the flow becomes very large, the CPU time needed to carry out the computation will be prohibitive. Two measures are adopted in this study to limit the number of vortices in the wake.

Firstly, a different, usually larger, core radius is used when discretising the interaction vortex than that employed for the vortices shed from the aerofoil surface. To simulate high Reynolds number flow around the aerofoil, the control zone should be very thin, of order $O(\frac{1}{\sqrt{Re}})$, to reflect the boundary layer near the body surface. Hence the core radius for the nascent vortices should also be of the order of the control zone height. If this core radius was to be used to discretise the interaction vortex with relatively large radius, then the number of the vortices would be excessively large.

Secondly, an amalgamation scheme is used for vortices in the wake which are far from the surface. Any two vortices with locations $\vec{x_j}$, $\vec{x_k}$ and strengths Γ_j, Γ_k respectively are merged into a new vortex with strength $\Gamma' = \Gamma_j + \Gamma_k$ and located at $\vec{x'} = (\Gamma_j\vec{x_j} + \Gamma_k\vec{x_k})/\Gamma'$, provided the effect of merging on the induced velocity at the body surface is very small[17], i.e.

$$\frac{|\Gamma_j\Gamma_k|}{|\Gamma_j + \Gamma_k|} \frac{|\vec{x_j} - \vec{x_k}|^2}{(D_0 + d_1)^{1.5}(D_0 + d_2)^{1.5}} \leq \epsilon \tag{18}$$

This scheme conserves both the total vorticity and linear moment of vorticity

Another possible method to further reduce the computational cost of the vortex method is to employ a fast summation algorithm, which has operational count $O(N_v)$ or $O(N_v log N_v)$ rather than $O(N_v^2)$ [19]. Such a scheme will be incorporated into the code in the near future.

4 RESULTS AND DISCUSSION

To show the feasibility and accuracy of the method, a number of BVI test cases have been calculated and the results compared with those obtained from other numerical and exprimental studies. The dominant mechanisms during a BVI event are also analysed and presented through illustration of the unsteady surface pressure distribution and loads, as well as the trajectory of the interaction vortex. For all the cases discussed here, the interaction vortex is introduced five chord lengths upstream of the leading edge and 160 surface panels are used to represent the contour of the aerofoil.

4.1 Comparison with other numerical results

Two typical cases with the same parameters as given in [10] are calculated for the interaction between a NACA 0012 aerofoil and a vortex modelled by the Rankine core. The strength Γ_v and the core radius R_v of the clockwise vortex are 0.2 and 0.1 respectively. For the first case, the interaction vortex is positioned slightly below the aerofoil ($Y_v=-0.26$), while for the second test case, the vortex approaches the aerofoil along the chordline ($Y_v=0$ or head-on case).

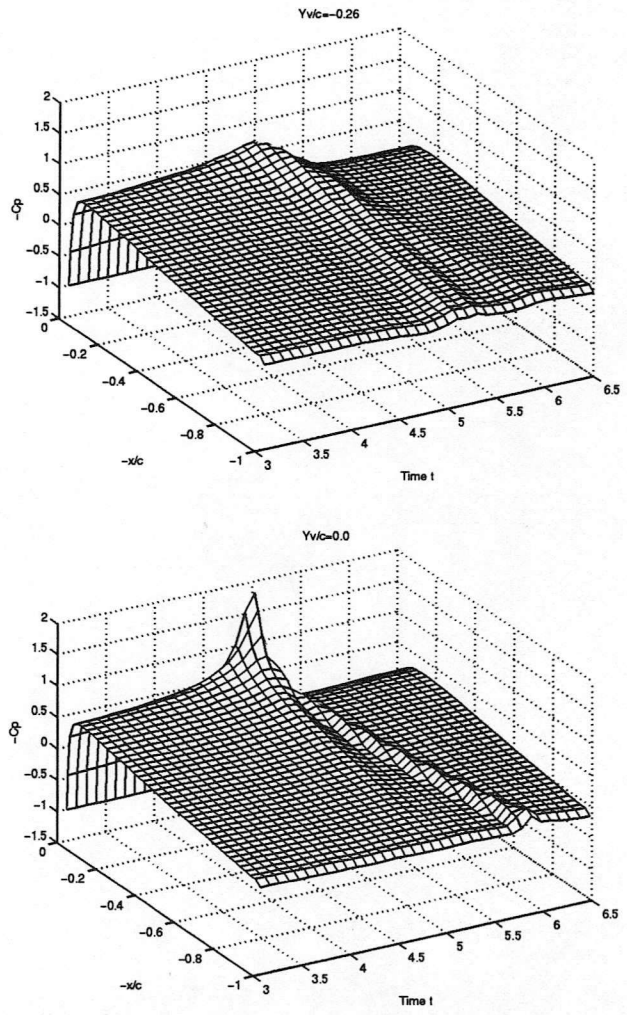

Figure 4. Surface pressure distribution

Figure 4 shows the development of the unsteady pressure distribution along the lower surface of the aerofoil for both cases, which indicates two distinct effects of the interaction vortex. Firstly, due to the effective incidence induced by the approaching vortex, a leading edge suction peak develops on the lower surface, reaching a maximum just before the vortex passes

the leading edge. Subsequently a rapid collapse of this peak occurs; while the magnitude of the suction peak is also affected by vortex induced changes in the local speed of the leading edge flow. Secondly, in these cases, as the vortex convects downstream along the surface of the aerofoil, it accelerates the flow close to the surface, and the resulting low pressure ridge is clearly visible.

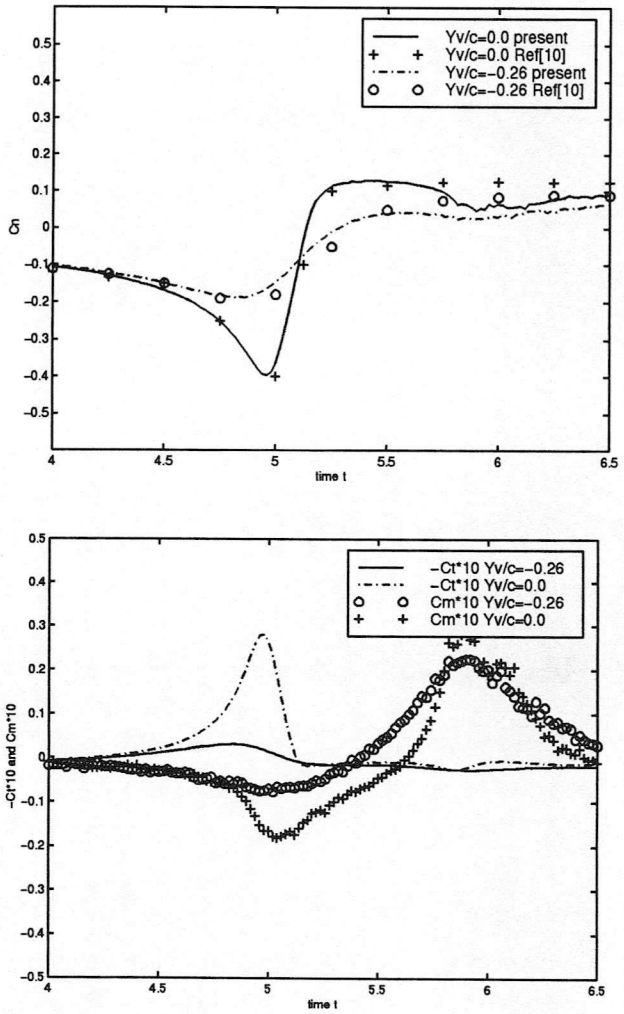

Figure 5. Evolution of the aerodynamic coefficients during the BVI

Figure 5 illustrates the integrated forces and quarter chord moment on the aerofoil during the interaction. The development and collapse of the C_n and C_t as well as the first peak in $C_{m\frac{1}{4}}$ can be explained by the effective incidence induced by the vortex, while the second and opposite peak in $C_{m\frac{1}{4}}$ is due to the extended moment arm as the low pressure wave travels along the aerofoil surface. In figure 5, the normal force coefficients from the unsteady panel method for both cases are also given, indicating good agreement between the two methods.

Another phenomenon associated with the close interaction, particularly for the head-on case, is the vortex striking the leading edge of the aerofoil and subsequently deforming and splitting into two fragments, see figure 6. The two separate parts of the vortex convect along the upper and lower surfaces with different velocities due to the mutual interaction between the passing vortex and the induced surface vorticity [20]. Moreover, due to the strong interaction between the oncoming vortex and the surface vorticity, a small local separation is predicted on the aft part of both surfaces where the adverse pressure gradient dominates. This phenomenon could not be predicted in the panel method, in which the vorticity is shed from the trailing edge

only, and is probably responsible for the small discrepancy in C_n between the two methods as the vortex travels off the aerofoil.

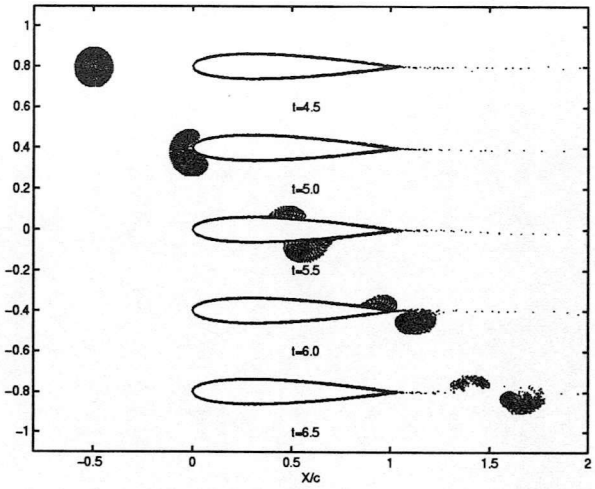

Figure 6. The trajectory of vortex particles for Y_v/c=0.0 case

4.2 Comparison with experimental data

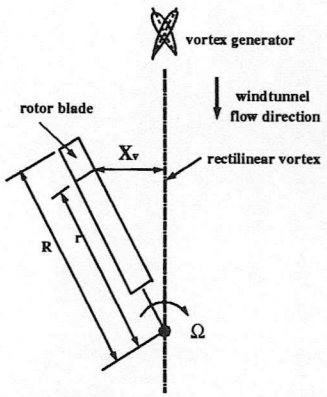

Figure 7. The set-up of the BVI test

The set up of the Glasgow BVI experiment [3][4][5] is sketched in figure 7. The interaction vortex is generated by two adjoining wings of NACA 0015 aerofoil section set at equal but opposite incidence, with the magnitude of the incidence controlling the vortex strength. The circumferential velocity distribution in the isolated interaction vortex is measured using both hot wire and PIV techniques, which gives an average value of the vortex strength Γ_v=5.8m^2/s and core radius R_v=25mm. These data are then used as the input parameters for the present simulation by employing the Scully vortex model. Although the flow around the rotating rotor is generally three-dimensional, it could be considered approximately two-dimensional as the rotor blade at zero angle of attack approaches and passes through the interaction region near the center line of the wind tunnel. In the following discussion, the data collected from the blade at r/R=0.785 are used for the comparison. The pressure and the integrated aerodynamic forces and moment are nondimensionalised using the tip velocity of the rotor which gives a nominal Reynolds number of 600,000.

Figure 8 illustrates the results for three typical BVI cases with different interaction heights, from which it can be seen that C_n and C_t agree well with the experiments, whereas there are some discrepancies in the $C_{m\frac{1}{4}}$ data for all cases as the vortex passes the aft part of the aerofoil surface. Due to the fact that the present prediction gives results consistent with the

mechanisms discussed in the previous section, the difference in $C_{m\frac{1}{4}}$ may be due to the relatively small number of pressure transducers (only twenty-six for this case) used for measuring the pressure distribution around the aerofoil, while the $C_{m\frac{1}{4}}$ value itself is very small and is therefore sensitive to the resolution of the pressure measuring points. Another possibility is the physical restrictions in placing the transducers at the trailing edge of the blade [5]. Nevertheless, further study is needed to clarify this aspect.

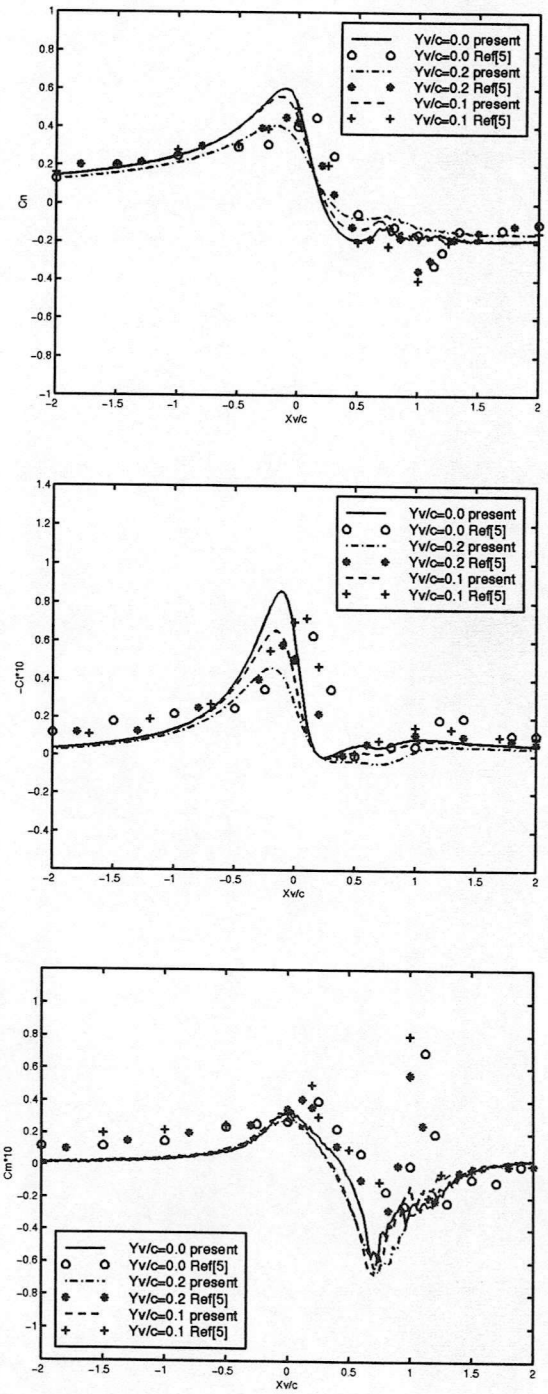

Figure 8. Evolution of aerodynamic coefficients during the BVI

In figure 9, two snapshots of the vortex passage for the head-on case are given, which also show that the interaction vortex is deformed and split into two parts which convect along the upper and lower surface at different speeds. On the aft part of the aerofoil surface, the vortex

induced local flow separation is clearly visible, which is consistant with the PIV results[4] for the same case.

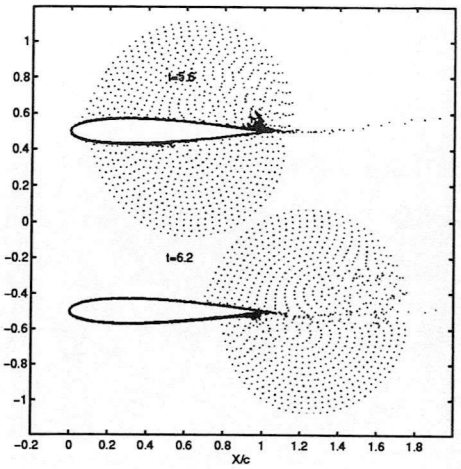

Figure 9. Trajectory of the vortex particles

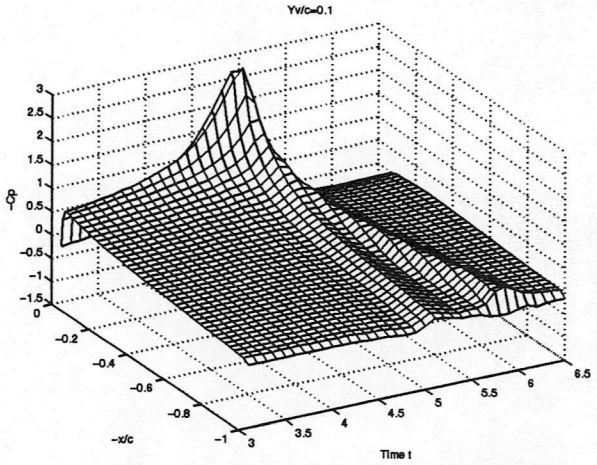

Figure 10. Surface pressure distribution

Finally, figure 10 gives the upper surface pressure distribution for the Y_v/c=0.1 case, which compares well with the experimental result given in [5]. The leading edge pressure suction peak and low pressure convection ridge are also well predicted.

5 CONCLUSIONS

This paper has presented numerical results for the parallel blade-vortex interaction problem, which shows the feasibility and flexibility of the grid-free discrete vortex method. A new method has been developed for calculating the velocity of the nascent vortices to avoid oscillations in the normal component. The dominant mechanisms during a BVI event, namely the effective angle of attack induced by the approaching vortex and the local effect due to passage of the vortex close by or around the surface, have been analysed using the unsteady C_p distribution together with images of the passing interaction vortex. For relatively strong BVI, such as the head-on interaction case, vortex-induced local flow separation, a phenomenon which has not been well documented in most BVI studies, has also been predicted in the present study.

Future work will include simulation of the interaction between an oncoming vortex and an aerofoil at high incidence and/or during dynamic stall, which represents a more complex vortex-vortex and vortex-body interaction problem.

ACKNOWLEDGEMENTS

The authors would like to thank C.A. Masson of Glasgow University for providing BVI experimental data and helpful discussion. The first author would also like to acknowledge the CVCP(UK) and the Faculty of Engineering at Glasgow University who provide sponsorships for study through the ORS scheme and the Engineering Scholarship respectively.

REFERENCES

[1] R. Padakannaya, 'Experimental study of rotor unsteady airloads due to blade vortex interaction', *NASA CR-1909*, (1971).

[2] F.X. Caradonna, G.H. Laub and C. Tung, 'An experimental study of the rotor-vortex interaction', *NASA TM-86005*, (1984).

[3] M.B. Horner, J.N. Stewart and R.A. Galbraith et al, 'Preliminary results from a particle image velocimetry study of blade-vortex interaction', *Aeronautical Journal*, **99**, 91–98, (1995).

[4] M.B. Horner, R.A. McD. Galbraith and F. Coton, 'Examination of vortex deformation during blade-vortex interaction', *AIAA J.*, **34**, 1188–1194, (1996).

[5] C.A. Masson, R.B. Green et al , 'An experimental investigation of a loaded blade-vortex interacting with single and twin vortices', *Proceedings of the Technical Specialists' Meeting for Rotorcraft Acoustics and Aerodynamics*, Williamsburg, Virginia, (1997).

[6] D.R. Poling, D.P. Telionis and L. Dadone, 'Blade-vortex interaction', *AIAA J.*, **28**, 694–699, (1989).

[7] R. Parthasarthy and K. Karamcheti, 'Aerodynamic sound generation due to vortex-aerofoil interaction', *AIAA paper 73-224*, (1973).

[8] C.Y. Chow and M.K. Huang, 'Unsteady flows about a Joukowski airfoil in the presence of moving vortices', *AIAA paper 83-0129*, (1983).

[9] A. Panaras, 'Numerical modelling of the vortex/aerofoil interaction', *AIAA J.*, **25**, 5–11, (1987).

[10] D.J. Lee and C.A. Smith, 'Effect of vortex core distortion on blade-vortex interaction', *AIAA J.*, **29**, 1355–1362, (1991).

[11] D.T. Mook and Bonian Dong, 'Perspective: Numerical simulations of wakes and blade vortex interaction', *J. Fluid Engineering*, **116**, 5–21, (1994).

[12] J.C. Hardin and S.L. Lamkin, 'Aerocoustic interaction of a distributed vortex with a lift Joukowski aerofoil', *AIAA paper 84-2287*, (1984).

[13] M.M. Rai, 'Navier-Stokes simulations of blade-vortex interaction using high-order accurate upwind scheme', *AIAA paper 87-0543*, (1987).

[14] H.E. Jones and F.X. Caradonna, 'Full potential modelling of blade-vortex interactions', *Vertica*, **12**, 129–145, (1988).

[15] A.T. Conlinsk, 'Modern helicopter aerodynamics', *Annu. Rev. Fluid Mech.*, **29**, 129–145, (1997).

[16] H.Q. Lin, M. Vezza and R.A.McD. Galbraith, 'Discrete vortex method for simulating unsteady flow around pitching aerofoils', *AIAA J.*, **35**, 494–499, (1997).

[17] P.R. Spalart, 'Vortex methods for separated flows', *NASA TM 100068*, (1988).

[18] A.J. Chorin, 'Numerical study of slightly viscous flow', *J. Fluid Mech.*, **57**, 785–798, (1973).

[19] I. Greengard and V. Rokhlin, 'A fast algorithm for particle simulations', *J. Comp. Phys.*, **73**, 325–333, (1987).

[20] T.L. Doligalski, C.R. Smith and J.D.A. Walker, 'Vortex interaction with walls', *Annu. Rev. Fluid Mech.*, **26**, 573–616, (1994).